Research Article

On the stress-induced photon emission from organism: I, will the scattering-limited delay affect the temporal course?

Daqing Piao[1]

Received: 20 November 2019 / Accepted: 17 August 2020 / Published online: 27 August 2020

Abstract
Much remains to be identified for the temporal course of stress-induced photon emission (PE) from organism following stress of various types including but not limited to light. Induced PE concerns surface light emission in excess of the baseline level of spontaneous ultraweak photon emission, in response to a localized or systematic stress via oxidative bursting. It is proposed that the surface emission of induced PE involves two causally sequential phases: a stress-transfer phase that transforms the stress to perturb photogenesis balanced at homeostasis and a photon-propagation phase that transmits the photons from the domain of perturbed photogenesis to surface emission. The traversing of induced PE photons from wherever the domains of photogenesis perturbation are in the organism following the stress to the surface must involve photon propagation of which the scattering will affect the photon lifetime. Induced PE is usually substantially retarded in occurrence or longer in duration with respect to the stress. In order to identify whether the time course of induced PE can be attributed entirely to the stress-perturbed photogenesis, Part I estimates the upper limit of the scattering-caused photon lifetime following photogenesis. The estimation of that upper limit is based on setting the photogenesis at the center of a spherical human-size tissue having an unrealistically strong tissue scattering. Time-resolved photon migration analysis reveals that the scattering-limited lifetime will not be greater than 100 ns at a human scale. The time course of induced PE reported thus suggests a much retarded and slower perturbation to photogenesis with respect to the time course of stress for manifesting the surface-observed induced PE. The theoretical insight, which may complement the soliton mechanism, also supports the exploration of entopic phenomena including phosphenes and negative afterimages via delayed PE. The subsequent Part II hypothesizes a few stress-transfer kinetic patterns feeding the photogenesis.

Keywords Ultraweak biophoton emission · Light propagation · Stress transfer · Diffusion kinetics

1 Introduction

Ultraweak photon emission (UPE) [1] concerns the spontaneous steady-state or stress-triggered varying emission of extremely weak light from an organism. UPE is sourced by the transition of excited biological molecules, mostly reactive oxygen species (ROS) and less commonly reactive nitrogen species (RNS) to lower-energy states [2]. ROS are generated at a fixed rate by oxidation–reduction reactions during cellular respiration, but are toxic to living cells [3]. UPE distinguishes itself from other forms of light emission such as fluorescence, phosphorescence and bioluminescence in terms of intensity, spectrum, spatial coherence and temporal rhythm [4–6], which collectively suggest under-resolved mechanistic origins. Many terms have appeared historically in referring to UPE phenomena: weak luminescence [7], low-level chemiluminescence [8], spontaneous chemiluminescence [9], biophoton(s)

✉ Daqing Piao, daqing.piao@okstate.edu | [1]School of Electrical and Computer Engineering, Oklahoma State University, Stillwater, OK 74078, USA.

emission [10, 11], ultra-weak bioluminescence [12], autoluminescence [13], spontaneous ultra-weak light emission [14], etc. The situation that a number of terms have been suggested to describe experimental observations speculated of the same underlying principles manifests that the slowly evolving understanding of UPE has yet to reach a consensus.

When in homeostasis, the cellular organism employs a variety of scavenging mechanisms to maintain the concentration of ROS at very low levels [3]. The luminescence intensity of the baseline spontaneous UPE of a living healthy organism is thus extremely low, at the orders of 100 s photons per square centimeter per second [11, 15] when measured on the surface, whereas the intra-organism intensity might be substantially higher [2]. The extremely weak illumination level makes UPE difficult to detect and unappealing for application. As a result, much controversy or uncertainty remains regarding the mechanistical, analytical and practical aspects of UPE. The hypothesized connection of UPE with consciousness and how cellular communication works [16, 17] further perplexes the exploration of UPE phenomena. Regardless of the not-yet-adequately-resolved biological origins and under-defined neurophysiological engagements of UPE, the UPE detection is in no doubt a matter of photon detection that has to be dictated by the principles of physics, including those determining photon propagations in biological tissue or organic medium and at the interface between two optically coupled media. The detection of UPE involves optimization of the optical, spectral, spatial and temporal configurations for photoelectronic instrument, similar to detecting any other weak illumination wherein increasing the sensitivity and suppressing the noise cross talk are essential [18]. UPE is reported to present a continuum spectrum covering the visible band and extending to near-infrared band [8, 10, 19–27]. Although the continuum spectral presentation of UPE is still elusive [27], studies have identified electron-related energy transitions of multiple types that occur in mitochondrial chemical chain reactions and result in broadband photon emissions of multiple local maximums that when combined may conform to the continuum spectrum of UPE [28]. The continuum spectrum of UPE renders the opportunity to control the spectral bandwidth of detection optics for both noise benefit and probing a specific spectral response of an organism in response to stress that can be externally controlled or modulated [29].

When living organisms become stressed by an external stimulation of various types including but not limited to light [30, 31], the concentration of ROS increases and induced photon emission (PE) in excess of the baseline level of spontaneous UPE is observed [32]. Induced change of the photon emissions provided much sought physiologically sound explanations to some very intriguing observations, including the entopic phenomena of phosphene and negative afterimage considered relating to lipid peroxidation [33–35]. The increase in photon counts in induced PE from an organism in excess of the baseline level of spontaneous UPE has been attributed mechanistically to oxidative burst caused by metabolic responses to an external stress or shock that disturbs the homeostasis [36–38]. Whatever the metabolic pathways prescribing the induced PE are, the photons of induced PE whose count is elevated from the baseline level of spontaneous UPE will appear on the tissue surface only after the onset of the stimuli, be it spatially localized or systematically applied or spectrally modulated, as is shown conceptually in Fig. 1a. In terms of the time course of an inducted phenomenon including but not limited to induced PE with

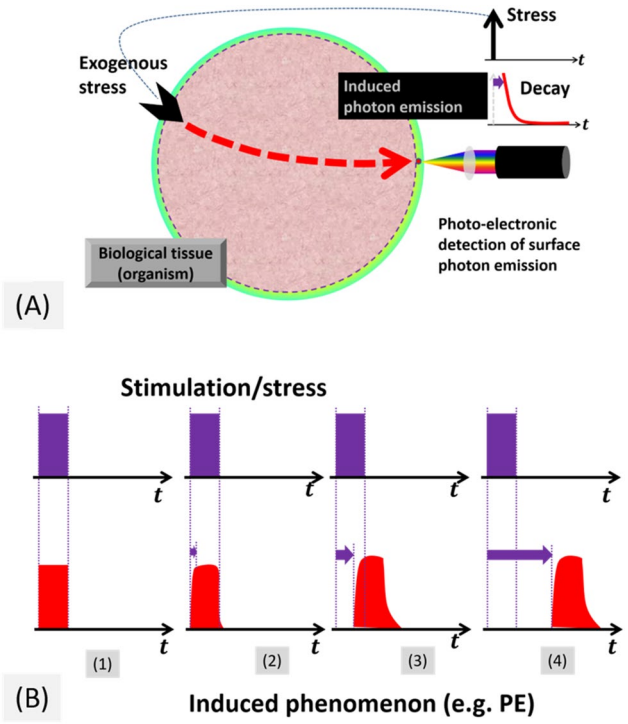

Fig. 1 **a** The elevation of the surface emission of UPE with respect to the baseline level of spontaneous emission occurs after the onset of an exogenous stress. There should have a non-instantaneous pathway to transfer the exogenous stress to the surface emission of more photons that delay in time with respect to the onset of exogenous stress and decay in intensity until reaching the baseline level of spontaneous emission, **b** we consider four cases possible for the temporal profile of an induced phenomenon (e.g., PE) with respect to the onset/removal of the stimulation/stress. (1) the induced phenomenon responds instantaneously to the stress; (2) the induced phenomenon appears instantaneously following the stress but there is a slower temporal change; (3) the induced phenomenon appears after the onset of the stress with a delay time less than the duration of the stress; and (4) the induced phenomenon appears after the removal of the stress

respect to the temporal profile of the stimulation or stress applied to the system that causes the phenomenon, four cases may be possible as shown in Fig. 1b. Case (1), the induced phenomenon responds instantaneously to the stress so the temporal profile of the induced phenomenon duplicates that of the stress without a delay at the onset or removal of the stress. Case (2), the induced phenomenon appears instantaneously following the stress but there is a slower temporal change to cause a rising phase at the onset and a falling phase at the removal of the stress. Case (3), the induced phenomenon appears after the onset of the stress with a delay time less than the duration of the stress. Case (4), the induced phenomenon appears after the removal of the stress.

Cases 1 and 2 may be hypothetical to the observed time course of induced PE with respect to the time course of the stress. However, the four hypothetical cases shown illustrate collectively that there should have two aspects of the temporal course of an induced phenomenon with respect to the temporal profile of the stimulation, which would apply equally to assessing the temporal course of induced PE that is usually delayed or slower with respect to the temporal course of stress. The first aspect of the temporal course of induced PE is when the change of surface photon count occurs with respect to the change of stress. This first aspect, *which is a time delay, retardation, or phase shift issue*, is represented by two specific responses: one is when the surface photon count changes (elevates) from the baseline level of spontaneous UPE in response to the onset of the stress, and the other is when the surface photon count changes (falls) from the induced steady-state level in response to the removal of the stress. The second aspect of the temporal course of induced PE is the time it takes for the change of the surface photon count to stabilize. This second aspect, *which is a kinetic decay or dynamic change issue*, is also represented by two specific responses: one is how long it takes for the surface photon count to change (elevate) from the baseline level of spontaneous UPE to the steady-state level of induction under a stress applied at a steady-state, and the other is how long it takes for the surface photon count to change (fall) from the steady-state level associated with the steady-state stress to the baseline level of spontaneous UPE after the stress is removed.

Without much exception, the existing reports of induced PE in response to stress of various types including but not limited to light have answered a lot of questions regarding the second aspect, or the kinetic decay issue, of the temporal course of induced PE. However, the first aspect, or the retarded or delayed occurrence of the induced PE with respect to the change of the stress has not been paid attention from the perspective of how that part of temporal course may affect the overall time course of induced PE. Should there be a delay of the photon appearance on surface that is caused solely by tissue optical properties that hamper light propagation in the absence of any secondary mechanism prolonging light presence in tissue, the tissue optical property-limited delay will affect both the temporal delay and kinetic decay that collectively compose the temporal course of the induced PE.

Of induced PE, the ones responding to photic stress or photo-illumination have registered the shortest device-specific delay time (which was bounded by the time-gap manageable between the removal of stress and the starting of photon acquisition without confounding the photon-detection due to the afterglow of the light illumination), a minimum of 8.5 μs after the removal of photo-illumination [39]. And the intensity of the initial peak of induced PE responding to photo-illumination can be several orders of magnitude stronger than the steady-state level of spontaneous UPE [40, 41]. Other types of external stimulation, such as chemical [30], mechanical [5], thermal/environmental [3], radiative [42], electrical [43] and magnetic [44] have shown to cause induced PE of relatively smaller change over the baseline level than the photic stimulation. Induced PE in response to non-photic stimulation is usually much slower in the decay kinetics and can last very long (up to several hours [45]) after the stress or shock was removed. Because induced PE responds to external stress through metabolic pathways that are linked to oxidative burst, controlling external stress can thus modulate the induced PE and suggestions have been made to use the decay kinetics of induced PE to probe the oxidative stress pathways [41, 46]. This viable application of induced PE with the promise to probe homeostasis is a challenge in the present, because the weak level of photon emission of induced PE (particularly when in association with non-photic stress) requires long acquisition time and highly sensitive photon-counting techniques in addition to the extreme care to the light tightness of the measuring environment. Exploring the application of induced PE is also difficult in the present, because much of the mechanistical (analytical and specific metabolic) association remains to be established between the various kinetic patterns of induced PE that can be measured and the external stress or shock that can be modulated.

The causal transitions of the external stimuli to the surface emission of induced PE photons may be unrealistically simplified but conceptually insightful as to follow two sequential processes: a stress-transfer process that triggers the photogenesis through pathways or mechanisms that are not resolved adequately but shall involve physiological or metabolic chain reactions, and a subsequent photon-propagation process that delivers the photon to tissue surface for photoelectronic detection that abides to pure optical principles. For induced PE photons produced inside

the tissue, the surface arrival of photons originating from wherever the sites of perturbation to photogenesis within the tissue are before being coupled to an outer interfacing layer [i.e., air] must involve a precedent stage of photon propagation within the tissue that would involve scattering by cellular and subcellular microstructures and absorption due to chromophores, if neglecting other types of light–tissue interactions. Therefore, the photon paths from the site of the perturbed photogenesis to the surface site will be modulated by tissue scattering, which will cause temporal spread or broadening of the photon's temporal profile even for an impulsive perturbation to photogenesis that responds instantaneously to an impulsive external stimulus (i.e., no delay between stress onset and photogenesis change). For a non-instantaneous process between the onset of external stimulus or stress and the perturbation to photogenesis that would source the induced PE, both the duration of the stress-transfer phase and the photon-propagation phase will delay or retard the surface appearance of photons with respect to the onset of the external stimulus. The temporal profile of the surface-measured induced PE in response to an external stimulus apparently will express the temporal characteristics of both of the two processes, namely the stress-transfer process and the photon-propagation process, and the length of the temporal retardation or the duration of the PE measured on tissue surface has to be no shorter than the longer temporal scale between the two phases. The well-known nonlinear soliton mechanism [47] that justifies the coherence and most common hyperbolic-decay patterns of induced PE may be intervened in one or both of the processes. Solitons may be formed in the stress-transfer phase to prolong the lifetime of the excited states, causing a delayed or slow photogenesis phase to produce the surface-emitted photons later and slower in time comparing to the onset or removal of stress. The soliton or soliton-alike state could also be involved in the photon-propagation phase, if the broadband nature of the induced photon could cause secondary photon emission by photon absorption/reemission to cause either higher intra-organism biophoton intensity [2] at a given moment or collectively prolong the effective lifetime of the photon in tissue when detected on the surface. Whichever the way that soliton states could be involved, it will not change the causality to dictate that the stress shall activate the change in photon production which will appear later as a change in the surface-emitted photon count.

Many studies have appeared for resolving the decay kinetics of induced PE, which is the second aforementioned factor affecting the temporal course of surface-measured induced PE. However, there has not been any work to this author's knowledge that has dedicated to appreciating how much temporal spread or broadening of surface-detected induced PE photons can be resulted from tissue scattering alone which directly affects the first afore-referenced factor and is also pertinent to the second afore-referenced factor in constituting the temporal course of induced PE. The lower limit of the temporal delay or retardation of induced PE with respect to the change in stress or external stimuli is trivial. The upper limit, however, affects how the delay or retardation of induced PE when arising with respect to the onset of stress and how the duration of induced PE when decaying with respect to the removal of stress can be interpreted for investigating the underlying mechanisms. The information concerning the temporal delay of photon propagation within tissue of organism that will be caused by light scattering is important to the identification of the dominating temporal cause of the induced PE, particularly for those scenarios associated with photic stimulation that has shown the fastest *decay* response and requires fast temporal gating for the recovery of decay kinetics. Should the temporal delay by tissue scattering be not negligible for the registration of induced PE, the duration and decay kinetics of induced PE shall be interpreted with full consideration of photon propagation in tissue, particularly for large tissue volume comparable in size to human and for an external stress that is off-site or systematic for any potential of health application. Should the temporal delay by tissue scattering be negligible in the registration of induced PE, any retardation and the duration over which the induced PE reveals a kinetic change will then be mechanistically governed by the process of states likely involving soliton formation that transfers the external stress (which is exogenous so open for modulation) to photogenesis (which is endogenous and hidden but is assessible and can be reconstructed by using surface measurements including tomographic approaches). A substantially later increase in surface-observed induced PE in comparison with what is possible by light propagation in tissue thus is hardly justifiable without a photon-production hike that could have occurred later than the onset of the stress. Similarly, a substantially longer reduction in surface-observed induced PE after the removal of the stress in comparison with what is accountable by light propagation delay in tissue may be accounted for only by a reduction in photon production that occurs later than the removal of the stress. A knowledge of such processes would thus be analytically informative to probing the underlying mechanism and projecting practical applications by using induced PE that can be correlated with modulable stress for the potential of coherence detection to improve the signal-to-noise yield and to complement the soliton mechanism in terms of quantitating the temporal spectral details of induced PE.

In this regard, this Part I attempts to estimate the upper limit of the temporal delay that is possible for the

surface-observed induced PE with respect to the photogenesis following a stress application. To assess this upper limit without losing the insight for practical applications pertaining the connection of oxidative stress with health conditions such as neurodegenerative disease [48], the analysis is performed for a human-size tissue and by assuming very strong tissue scattering to present long delay of the surface emission of photon when originating from the deepest interior of tissue. The solution of the temporal spread of photon propagation in response to a spatially and temporally impulsive photon source is derived for the spherical tissue domain whose size is several orders of magnitude greater than the photon scattering pathlength. The solution is then numerically evaluated for tissue domain with significantly exaggerated scattering conditions comparing to what is realistic for a tissue, in order to assess how the maximal temporal spread of photon diffusion measured at the tissue surface that can be caused by tissue scattering compares with the known observation of the device-specific delay or retardation that occurs after the removal of the stress. The upper bound of the temporal delay of photon with the spectral relevancy to PE due to tissue scattering is assessed analytically by solving time-resolved photon diffusion over a spherical tissue domain of 40 cm in diameter that approximates the cross-sectional size of human body and with a reduced scattering coefficient as strong as 500 cm^{-1}, by also implementing a boundary condition common for assessing photon remission from tissue that interfaces with air.

2 Temporal propagation of light of spectral relevancy to induced PE in a spherical air-bounding tissue domain: analytical principle

The greater the photon path in the scattering tissue domain is and the stronger the tissue scattering is, the longer the temporal spread of the photon prorogation becomes. To assess the maximal temporal delay or broadening of photons in tissue due to scattering in a volume applicable to human scale for the potential of health application, it is necessary to assume a large tissue volume and a strong tissue scattering. The light propagation in bulk tissue is accurately described by the radiative transfer equation [49]. In assessing the maximal temporal spread of photon propagation that can be caused by tissue scattering alone, the photon diffusion approximation [50] to the radiative transfer equation will be implemented as that accurately describes diffuse photon propagation in scattering biological tissues over a distance that is substantially longer than the mean scattering pathlength of the photon in tissue.

An important aspect of the physical principles shared by detecting induced PE or spontaneous UPE, referred to as photons of UPE nature, with other light acquisition scenarios that must be cared about for photon detection is the "boundary effect" that governs both ballistic and non-ballistic light transmission from one medium to the other. A likely example of "boundary effect" on detecting photons of UPE nature was demonstrated by Nakamura and Hiramatsu [51] in acquiring biophotons from human hand by using a photomultiplier tube (PMT). When there was an air layer between the palm and the glass window of the PMT, about 100 photon counts per second was obtained. When mineral oil was used to buffer the hand with the glass window of the PMT, about 200 photon counts per second was obtained. This was approximately twice as much in comparison with the former one. Similar level of enhancement of the photon counts was obtained also by water buffering of the PMT glass window with the palm (it was not clear whether the cathode potential of PMT would have been affected by the buffering). The results, after accounting for the difference in dark count among the different configurations, indicated that the contact of the hand with the oil did not lead to an increase in the photon emission of the hand by a chemical reaction and that the emission from the inside of the skin certainly existed. The enhancement of photon passage from tissue to PMT light collection chamber at the presence of a buffer layer of mineral oil was attributed to better matching of the refractive index across the boundaries that the photons had to pass. Regardless of where the photons were generated (i.e., the site of photogenesis) within the tissue, sandwiching the tissue and the glass window of the PMT with a layer having an intermediate refractive index to enhance the collection of UPE photon is, unmistakably, a presentation of the boundary-value principle of light transmission between two media. Were the photons of UPE nature generated on or extremely close to (shorter than a few scattering pathlengths) the surface of the tissue, the transmission of those photons from tissue to the outer interfacing layer, be it mineral oil or the air between the tissue and the PMT glass window, will be primarily ballistic or quasi-ballistic and so the transmission of photons from the superficial tissue layer to the detector is then affected primarily by the Fresnel refraction. Were the photons of UPE nature produced inside the tissue, the surface arrival of UPE photons from wherever the sites of photogenesis within the tissue are before being coupled to the outer interfacing layer must involve diffuse photon propagation within the tissue due to scattering by cellular and subcellular microstructures and absorption by chromophores, among other light–tissue interactions.

In the following sections, the time-resolved diffusion of light with spectral relevancy to induced PE or

spontaneous UPE (i.e., in the VIS/NIR band of biological window for which the photon diffusion analysis is conventional) is treated with spherical Eigenfunction decomposition, Laplace transformation and necessary approximation to facilitate numerical evaluation of the problem in a spherical tissue geometry with the pertinent boundary condition. The tissue geometry for the surface emission of photon concerns a spherical tissue volume with the photo-sourcing assumed to occur deep in the center that aligns with the objective to assess the maximal temporal delay caused by scattering. The spherical tissue geometry is indubitably an overly simplified representation of the tissue domain from which the induced PE could be measured on the surface. However, a spherical tissue domain would be more applicable to the potential of health application than the much simpler semi-infinite tissue geometry. And the placement of a photon source deep in the center of the spherical tissue volume is necessary for the estimation of the longest time delay with respect to the moment of photogenesis for surface measurement that has a dynamic range of the photon counts reasonable for instrument detection. The geometry as is approached by having the photon source deep in the center of the spherical tissue domain also differs from the common reflectance configuration upon a semi-infinite tissue geometry whereby photons are injected into the tissue and detected from the tissue on the same tissue–air interface. The tissue is assumed to be optically homogeneous for simplicity. So the tissue properties affecting spectral light propagation including absorption coefficient and reduced scattering coefficient are the properties averaged over a bulk volume of tissue to manage analytical treatment. Analysis of the problem in tissue that is optically inhomogeneous can be done by using numerical techniques such as time-domain finite element approach [52]. Further, cellwise or molecular-size analysis of the light propagation delay caused by scattering may not be prohibitive, but the analytical and computational costs will be humongous and the outcomes will have to be assembled over a bulk organism as big as human size for health potential, whereby the volume averaging will make the use of bulk-tissue optical properties valid unless the sites of photogenesis need to be spatially resolved and that does not seem to be possible without more analytical and mechanistical discoveries to resolve the pathways that could be both complex and numerous. Since an optical inhomogeneity would complicate the photon-propagation phase to increase the frequency complexities of the point-spread function that would effectively narrow the temporal spreading profile, the maximal temporal delay estimated for an optically inhomogeneous tissue that can be measured by an instrument of limited dynamic range would be less than that for an optically homogenous tissue having the same global optical properties as the former. For this reason, the analysis on optically homogeneous tissue would suffice the need to estimate the maximal temporal spread of the propagation of the induced PE from the site of photogenesis to surface site of observation.

The equation of time-resolved diffusion of a light of UPE spectral relevancy (in the Vis–NIR spectral band) in a highly scattering biological tissue at a specific wavelength is as the following [53]:

$$\nabla^2\hat{\Psi}(\vec{\chi},t)-\frac{\mu_a(\vec{\chi})}{D(\vec{\chi})}\hat{\Psi}(\vec{\chi},t)-\frac{1}{D(\vec{\chi})\cdot c}\frac{\partial\hat{\Psi}(\vec{\chi},t)}{\partial t}=-\frac{1}{D(\vec{\chi})}q(\vec{\chi},t) \tag{1}$$

where $\hat{\Psi}(\vec{\chi},t)$ is the photon fluence rate (unit: $mm^{-2}\ sr^{-1}$) at a spatial position $\vec{\chi}$ and a temporal point t, $\mu_a(\vec{\chi})$ is the absorption coefficient (unit: mm^{-1}), $D(\vec{\chi})=\{3[\mu_a(\vec{\chi})+\mu_s'(\vec{\chi})]\}^{-1}$ is the diffusion coefficient (unit: mm) with $\mu_s'(\vec{\chi})$ being the reduced scattering coefficient (unit: mm^{-1}), c is the speed of light (unit: $mm\ s^{-1}$) in medium and $q(\vec{\chi},t)$ is the source or the photon density (unit: $mm^{-3}\ sr^{-1}$). For a homogeneous and boundless medium, the equation of the Green's function of (1) becomes the following:

$$\nabla^2\hat{\Psi}_{\text{inf}}(\vec{\chi}',t'|\vec{\chi},t)-\frac{\mu_a}{D}\hat{\Psi}_{\text{inf}}(\vec{\chi}',t'|\vec{\chi},t)-\frac{1}{Dc}\frac{\partial\hat{\Psi}_{\text{inf}}(\vec{\chi}',t'|\vec{\chi},t)}{\partial t}=-\frac{1}{D}\cdot\delta(\vec{\chi}-\vec{\chi}')\cdot\delta(t-t') \tag{2}$$

where the subscript "inf" represents "infinite geometry" or boundless medium. The $\hat{\Psi}_{\text{inf}}(\vec{\chi}',t'|\vec{\chi},t)$ of Eq. (2) corresponds to the photon fluence rate at a spatial position of $\vec{\chi}$ and a temporal position of t, in response to an impulsive source stimulation of unitary intensity that occurs at a spatial position $\vec{\chi}'$ and a temporal point t'. The temporal profile of $\hat{\Psi}_{\text{inf}}(\vec{\chi}',t'|\vec{\chi},t)$ is thus the temporal impulse response of the tissue medium, which when convolved with the temporal profile of any source produces the composite temporal response of the medium to that actual source.

Since photon diffusion through the biological system has to be causal, we must have $\hat{\Psi}(\vec{\chi}',t'|\vec{\chi},t)=0$ for $t<t'$ for a previously source-less medium. For a medium that has a steady-state baseline emission of photons, any change in the photon emission from the steady-state baseline has to be causal as well. We thus use $\hat{\Psi}(\vec{\chi}',0|\vec{\chi},t)$ to represent the photon fluence rate at a time $t\geq 0$ in response to a source injected (or appearing) at $t'=0$, by normalizing the initial condition to $\hat{\Psi}(\vec{\chi}',0|\vec{\chi},t)\big|_{t=0}=0$ without losing the generality.

An organism under exogenous stress that emits induced PE photons for acquisition at the surface of the organism is illustrated schematically in Fig. 2. The organism or biological tissue for the model purpose is simplified as a spherical volume, which is referred to as SOMA, of radius R_0. An arbitrary photon source q (unit: cm^{-3} sr^{-1}) responsible for surface emission of photon is set at $(R_{phot}, \theta', \phi')$. The site for surface photodetection is assumed to be (R_o, θ, ϕ).

It must be noted that the surface photon emission of UPE spectral relevancy as a result of complex spatial extension or temporal profile of the photon production within the tissue volume can only be developed when the photon emission in response to a single and simple source is accurately resolved, which is the scope of this work. The analysis that follows thus is restricted to the photon emission at the surface site of (R_o, θ, ϕ) in response to a single source at $(R_{phot}, \theta', \phi')$. With regard to the effect on photon fluence rate by the tissue–air boundary, the photon fluence rate is set zero at a boundary extrapolated at a distance away from the physical boundary of tissue—the so-called extrapolated zero boundary [54] that is shown to be accurate for boundary-value problems of photon diffusion. For any source within the tissue medium, the extrapolated boundary condition introduces an "image" of the source by mirroring the source with respect to the extrapolated zero boundary that is concentric with and at a radial distance of $R_b = 2AD$ outward from the physical boundary [55] where $A = (1 + \xi)/(1 - \xi)$, $\xi = -1.440n^{-2} + 0.710n^{-1} + 0.668 + 0.0636n$ and n is the refractive index of the air-bounding tissue. The composite photon fluence rate at the extrapolated boundary that results from both the physical source in the tissue medium and the image of the physical source with respect to the extrapolated boundary is set to zero. Subsequently, the composite photon fluence rate at the tissue medium surface, which is positive, is quantifiable by using the same two sources as governed by the uniqueness property of boundary value problems.

For a photogenic source $q(\vec{\chi}', 0)$ located off-center at $(R_{phot}, \theta', \phi')$, the geometric symmetry determines that the image of it with respect to the extrapolated boundary must locate along the same radial direction of it. The source $\hat{q}(\vec{\chi}', 0)$ and its image with respect to the extrapolated

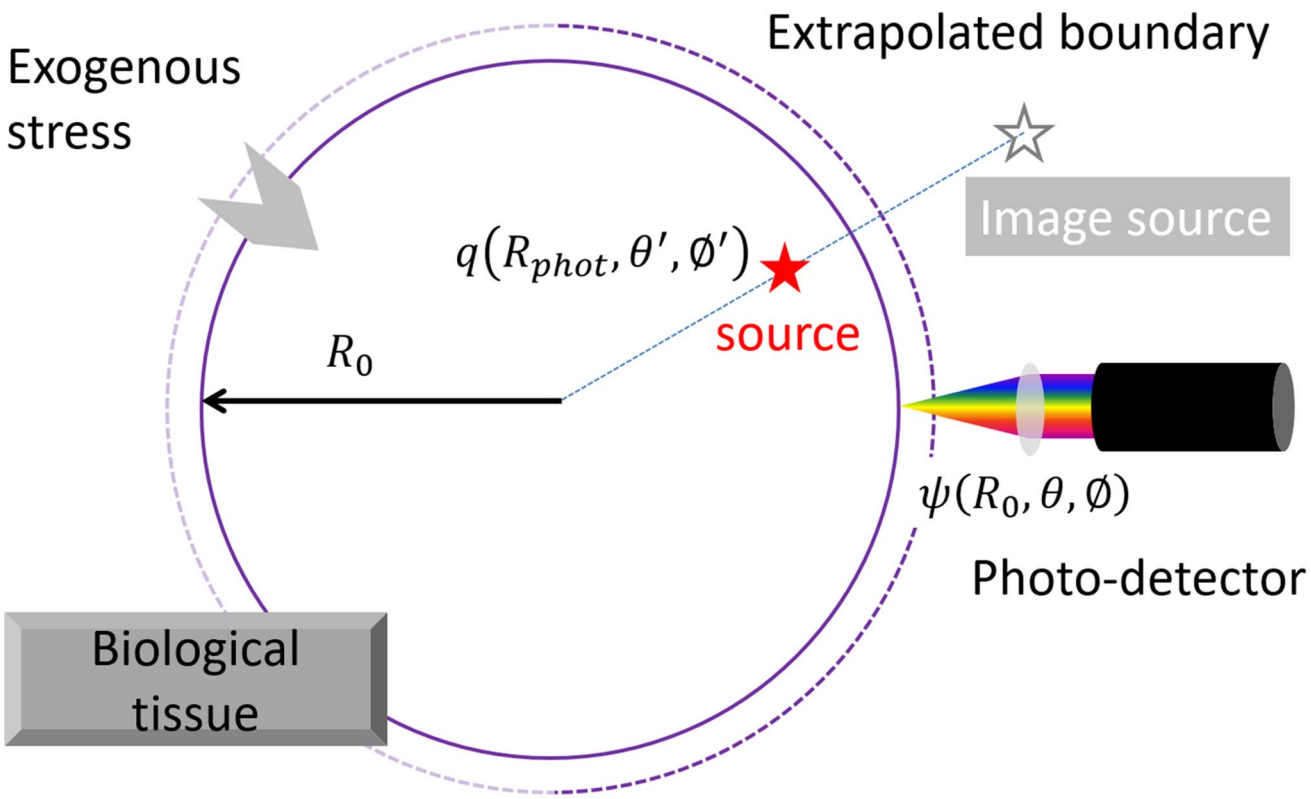

Fig. 2 The acquisition of surface emission of UPE photons from a spatially impulsive photogenic source located inside an organism is illustrated for a spherical geometry with a radius of R_0. The spatially impulsive photogenic source of intensity q is assumed to locate at $(R_{phot}, \theta', \phi')$. Surface measurement of the photon emission occurs at (R_0, θ, ϕ). An imaginary boundary away from the physical tissue–air boundary is assumed for applying the boundary condition approximated to assess the surface emission of photons after propagating with the scattering tissue medium

boundary collectively set zero the photon fluence rate (as well as its LT) on the extrapolated boundary represented by Ω:

$$\hat{\Psi}(\vec{\chi}',0|\vec{\chi},t) = \hat{\Psi}_{\text{phot}}\Big|_{\text{ext}}(\vec{\chi}',0|\vec{\chi},t) + \hat{\Psi}^{\text{imag}}_{\text{phot}}\Big|_{\text{ext}}(\vec{\chi}',0|\vec{\chi},t) = 0, \quad \text{for} \quad \vec{\chi} \in \Omega \tag{3}$$

3 Approximated solution of the time-resolved photon fluence rate of spectral relevancy to induced PE at the surface of a large spherical tissue volume in response to an interior source

The Laplace transform (LT) of Eq. (2) with respect to t when $t' = 0$ leads to the following:

$$\nabla^2\hat{\Psi}_{\text{inf}}(\vec{\chi}',0|\vec{\chi},s) - \frac{s+\mu_a c}{Dc}\hat{\Psi}_{\text{inf}}(\vec{\chi}',0|\vec{\chi},s) = -\frac{1}{D}\cdot\delta(\vec{\chi}-\vec{\chi}') \tag{4}$$

The solution of Eq. (4), $\hat{\Psi}_{\text{inf}}(\vec{\chi}',0|\vec{\chi},s)$ is the "free-space" solution in the frequency domain as associated with a source–detector pair in a homogeneous medium of infinite geometry. The solution to Eq. (4) when expressed with the use of spherical harmonics is [55]:

$$\hat{\Psi}_{\text{inf}}(\vec{\chi}',0|\vec{\chi},s) = \frac{1}{D}(\hat{\mu}^s_{\text{eff}})\sum_{l=0}^{\infty}\left[i_l(\hat{\mu}^s_{\text{eff}}r_<)\cdot k_l(\hat{\mu}^s_{\text{eff}}r_>)\right]\sum_{m=-l}^{l}\left[Y^*_{lm}(\theta',\phi')\cdot Y_{lm}(\theta,\phi)\right] \tag{5}$$

where i_l and k_l are, respectively, the lth-order modified spherical Bessel function of the first and the second kinds, $r_<$ and $r_>$ are, respectively, the smaller and greater radial coordinates of the source and the detector or the field position, Y_{lm} is the spherical harmonics function, and $\hat{\mu}^s_{\text{eff}}$ is defined as:

$$\hat{\mu}^s_{\text{eff}} = \sqrt{\frac{\mu_a}{D}+\frac{s}{Dc}} = \sqrt{s+\mu_a c}\frac{1}{\sqrt{Dc}} \tag{6}$$

Note that the $\hat{\Psi}_{\text{inf}}(\vec{\chi}',0|\vec{\chi},s)$ of Eq. (5) can also be expressed in a much simpler form in spherical coordinates, which is the commonly presented solution of equation of Eq. (4), as

$$\hat{\Psi}_{\text{inf}}(\vec{\chi}',0|\vec{\chi},s) = \frac{1}{4\pi D}\frac{1}{|\vec{\chi}-\vec{\chi}'|}\exp\left(-\sqrt{s+\mu_a c}\frac{1}{\sqrt{Dc}}|\vec{\chi}-\vec{\chi}'|\right) \tag{7}$$

The inverse LT of Eq. (7) can be found according to a LT pair [56] of $t^{-3/2}\exp(-a/4t) \overset{\text{LT}}{\Leftrightarrow} 2\sqrt{\pi}\left(1/\sqrt{a}\right)\exp\left(-\sqrt{as}\right)$, the frequency-shifting property of LT and the time delay or phase-shifting properties of LT. Thus, the time-resolved photon fluence rate in a homogeneous boundless medium which is the inverse LT of $\hat{\Psi}_{\text{inf}}(\vec{\chi}',0|\vec{\chi},s)$ is obtained as [56]

$$\hat{\Psi}_{\text{inf}}(\vec{\chi}',0|\vec{\chi},t) = \frac{c}{(4\pi)^{3/2}}\frac{1}{[Dct]^{3/2}}\cdot\exp\left[-\mu_a ct\right]\cdot\exp\left(-\frac{1}{4Dct}|\vec{\chi}-\vec{\chi}'|^2\right) \tag{8}$$

Based on Eq. (8), the LT of the photon fluence rate associated with the photogenic source $\hat{q}(\vec{\chi}',0)$ and evaluated on the extrapolated boundary, for which the source locates at $r_< = R_{\text{phot}}$ and the field point locates at $r_> = R_0 + R_b$, is

$$\hat{\Psi}_{\text{phot}}\Big|_{\text{ext}}(\vec{\chi}',0|\vec{\chi},s) = \frac{1}{D}(\hat{\mu}^s_{\text{eff}})\sum_{l=0}^{\infty}\left\{i_l\left[\hat{\mu}^s_{\text{eff}}\cdot(R_{\text{phot}})\right]\cdot k_l\left[\hat{\mu}^s_{\text{eff}}(R_0+R_b)\right]\right\}\cdot\sum_{m=-l}^{l}\left[Y^*_{lm}(\theta',\phi')\cdot Y_{lm}(\theta,\phi)\right] \tag{9}$$

where the notation "$\text{left}\Big|_{\text{right}}$" indicates that the evaluation is associated with the "left" as the source and on the "right" as the field position. Note that any lth order (or moment) of the photogenic source $\hat{q}(\vec{\chi}',0)$ has the same unitary intensity. Similarly, the LT of the photon fluence rate associated with the image of the photogenic source and evaluated on the extrapolated zero boundary, for which the source now locates at a radial position of a to-be-determined $r_>$ and the detector locates at $r_< = R_0 + R_b$, is

$$\hat{\Psi}^{\text{imag}}_{\text{phot}}\Big|_{\text{ext}}(\vec{\chi}',0|\vec{\chi},s) = \frac{1}{D}(\hat{\mu}^s_{\text{eff}})\sum_{l=0}^{\infty}q^*_l\cdot\left\{i_l\left[\hat{\mu}^s_{\text{eff}}\cdot(R_0+R_b)\right]\cdot k_l\left[\hat{\mu}^s_{\text{eff}}r_>\right]\right\}\cdot\sum_{m=-l}^{l}\left[Y^*_{lm}(\theta',\phi')\cdot Y_{lm}(\theta,\phi)\right] \tag{10}$$

where the q^*_l terms are dependent upon the order (or moment) l. Based on the essence of "image-source" [55, 56], the two unknown terms q^*_l and $r_>$ associated with the lth-order (or moment) "image" source (the k_l component) can be expressed by a single unknown term q_l associated with the same order (or moment) of the actual photogenic source $\hat{q}(\vec{\chi}',0)$ located within the tissue at $(R_{\text{phot}},\theta',\phi')$ (the i_l component), as the following:

$$q_l^* \cdot k_l\left[\hat{\mu}_{\text{eff}}^s r_>\right] = q_l \cdot i_l\left[\hat{\mu}_{\text{eff}}^s\left(R_{\text{phot}}\right)\right] \tag{11}$$

Applying Eqs. (9)–(11) to the condition of extrapolated zero boundary defined by Eq. (3) leads to

$$q_l = -\frac{k_l\left[\hat{\mu}_{\text{eff}}^s\left(R_0+R_b\right)\right]}{i_l\left[\hat{\mu}_{\text{eff}}^s\left(R_0+R_b\right)\right]} \quad l = 0, 1, 2, \ldots \tag{12}$$

Now for the LT of photon fluence rate associated with the photogenic source at $\left(R_{\text{phot}}, \theta', \phi'\right)$, but evaluated at a field point between the body boundary and the extrapolated zero boundary, the source still locates at $r_< = R_{\text{phot}}$ but the detector or the field point locates at $r_> = R_0 + \Delta r$, where $\Delta r \in \left[0, R_b\right]$ (a field point on the body boundary simply corresponds to $r_> = R_0$ or $\Delta r = 0$). For the LT of the photon fluence rate associated with the image of the photogenic source and also evaluated at a field point between the body boundary and the extrapolated zero boundary, the field point now locates at $r_< = R_0 + \Delta r$ and the source terms are known through Eqs. (10) and (11). Collectively, the composite LT of the photon fluence rate originating from a photogenic source at $\left(R_{\text{phot}}, \theta', \phi'\right)$ and sensed by a detector or field point at $\left(R_0 + \Delta r, \theta, \phi\right)$ between the body boundary and the extrapolated boundary becomes:

$$\begin{aligned}
\hat{\Psi}_{\text{SOMA}}\left(\vec{\chi}', 0|\vec{\chi}, s\right) &= \hat{\Psi}_{\text{phot}}\Big|_{\text{ext}}\left(\vec{\chi}', 0|\vec{\chi}, s\right) + \hat{\Psi}_{\text{phot}}^{\text{imag}}\Big|_{\text{ext}}\left(\vec{\chi}', 0|\vec{\chi}, s\right) \\
&= \frac{1}{D}\left(\hat{\mu}_{\text{eff}}^s\right)\sum_{l=0}^{\infty} i_l\left[\hat{\mu}_{\text{eff}}^s\left(R_{\text{phot}}\right)\right] \cdot k_l\left[\hat{\mu}_{\text{eff}}^s\left(R_0+\Delta r\right)\right]\sum_{m=-l}^{l} Y_{lm}^*\left(\theta', \phi'\right) Y_{lm}(\theta, \phi) \\
&\quad - \frac{1}{D}\left(\hat{\mu}_{\text{eff}}^s\right)\sum_{l=0}^{\infty} \cdot i_l\left[\hat{\mu}_{\text{eff}}^s\left(R_0+\Delta r\right)\right] i_l\left[\hat{\mu}_{\text{eff}}^s\left(R_{\text{phot}}\right)\right] \cdot \frac{k_l\left[\hat{\mu}_{\text{eff}}^s\left(R_0+R_b\right)\right]}{i_l\left[\hat{\mu}_{\text{eff}}^s\left(R_0+R_b\right)\right]}\sum_{m=-l}^{l} Y_{lm}^*\left(\theta', \phi'\right) Y_{lm}(\theta, \phi) \\
&= \frac{1}{D}\left(\hat{\mu}_{\text{eff}}^s\right)\sum_{l=0}^{\infty} i_l\left[\hat{\mu}_{\text{eff}}^s\left(R_{\text{phot}}\right)\right] \cdot k_l\left[\hat{\mu}_{\text{eff}}^s\left(R_0+\Delta r\right)\right]\sum_{m=-l}^{l} Y_{lm}^*\left(\theta', \phi'\right) Y_{lm}(\theta, \phi) \\
&\quad \left\{1 - \frac{i_l\left[\hat{\mu}_{\text{eff}}^s\left(R_0+\Delta r\right)\right]}{k_l\left[\hat{\mu}_{\text{eff}}^s\left(R_0+\Delta r\right)\right]}\frac{k_l\left[\hat{\mu}_{\text{eff}}^s\left(R_0+R_b\right)\right]}{i_l\left[\hat{\mu}_{\text{eff}}^s\left(R_0+R_b\right)\right]}\right\}
\end{aligned} \tag{13}$$

Equation (13) contains two parts: the "1" in the global bracket within the summation represents the infinite-medium contribution to the LT of the photon fluence rate associated with the photogenic source $\hat{q}\left(\vec{\chi}', 0\right)$ that can be expressed by the alternative simple form of Eq. (7); and the other term in the bracket is the scaling of the infinite-medium contribution to the LT of the photon fluence rate by the image of the photogenic source $\hat{q}\left(\vec{\chi}', 0\right)$ with respect to the former one. By using some analytics of the modified spherical Bessel function and Eq. (12), it is possible to convert Eq. (13) to the following form [55]

$$\begin{aligned}
\hat{\Psi}_{\text{SOMA}}\left(\vec{\chi}', 0|\vec{\chi}, s\right) &= \frac{1}{4\pi D}\frac{1}{\left|\vec{X} - \vec{X}_{\text{phot}}'\right|}\exp\left(-\hat{\mu}_{\text{eff}}^s\left|\vec{X} - \vec{X}_{\text{phot}}'\right|\right) \\
&\cdot\left\{1 - \frac{I_{l+1/2}\left[\hat{\mu}_{\text{eff}}^s\left(R_0+\Delta r\right)\right]}{K_{l+1/2}\left[\hat{\mu}_{\text{eff}}^s\left(R_0+\Delta r\right)\right]}\frac{K_{l+1/2}\left[\hat{\mu}_{\text{eff}}^s\left(R_0+R_b\right)\right]}{I_{l+1/2}\left[\hat{\mu}_{\text{eff}}^s\left(R_0+R_b\right)\right]}\right\}
\end{aligned} \tag{14}$$

where $I_{l+\frac{1}{2}}$ and $K_{l+\frac{1}{2}}$ are, respectively, the $\left(l+\frac{1}{2}\right)$th-order modified Bessel function of the first and the second kinds. This work considers an organism of the size of a human as that will produce much longer delay of photons measured at the surface in comparison with a small organism like a cell or tumor, for the purpose of assessing the upper limit of the temporal spread of photons of UPE spectral relevancy that can be caused by tissue scattering alone. If the temporal spread of the photon in this large SOMA is substantially smaller than the temporal scale of the induced PE known to the current experimental records, so is the temporal spread of the propagation of UPE photon in any organisms reported. For a human-sized tissue domain, it is convenient to have an R_0 (i.e., 10 cm) that is substantially greater than ten times of the magnitude of $1/\hat{\mu}_{\text{eff}}^s$ to have the second term in the bracket of Eq. (14) approximated by

$$\begin{aligned}
&\frac{I_{l+1/2}\left[\hat{\mu}_{\text{eff}}^s\left(R_0+\Delta r\right)\right]}{K_{l+1/2}\left[\hat{\mu}_{\text{eff}}^s\left(R_0+\Delta r\right)\right]}\frac{K_{l+1/2}\left[\hat{\mu}_{\text{eff}}^s\left(R_0+R_b\right)\right]}{I_{l+1/2}\left[\hat{\mu}_{\text{eff}}^s\left(R_0+R_b\right)\right]} \\
&\quad = \exp\left[-2\hat{\mu}_{\text{eff}}^s\left(R_b - \Delta r\right)\right]
\end{aligned} \tag{15}$$

which will change Eq. (14) to a simple form of

$$\begin{aligned}
\hat{\Psi}_{\text{SOMA}}\left(\vec{\chi}', 0|\vec{\chi}, s\right) &= \frac{1}{4\pi D}\frac{1}{\left|\vec{X} - \vec{X}_{\text{phot}}'\right|}\exp\left(-\hat{\mu}_{\text{eff}}^s\left|\vec{X} - \vec{X}_{\text{phot}}'\right|\right) \\
&\quad \left\{1 - \exp\left[-2\hat{\mu}_{\text{eff}}^s\left(R_b - \Delta r\right)\right]\right\}
\end{aligned} \tag{16}$$

Equation (16) that is associated with the photogenic source $\hat{q}(\vec{\chi}', 0)$ facilitates the condition of producing zero composite LT of the photon fluence rate at the extrapolated zero boundary whereupon $\Delta r = R_b$. Equation (16) also determines that the LT of the photon fluence rate associated with the photogenic source $\hat{q}(\vec{\chi}', 0)$ decreases monotonically away from the body boundary up to the extrapolated zero boundary, which is intuitively sound. Similar patterns hold for the photon fluence rate, since LT is a linear transformation. It can be demonstrated that Eq. (16) also applies to a source at the center of a spherical tissue domain that is significantly greater than the reduced scattering pathlength.

By using Eq. (7), Eq. (16) evolves to the following:

$$\begin{aligned}\Psi_{\mathrm{SOMA}}(\vec{\chi}', 0|\vec{\chi}, s) &= \frac{1}{4\pi D}\frac{1}{\left|\vec{X}-\vec{X}'_{\mathrm{phot}}\right|}\left\{\begin{array}{c}\exp\left(-\hat{\mu}^{s}_{\mathrm{eff}}\left|\vec{X}-\vec{X}'_{\mathrm{phot}}\right|\right)\\ -\exp\left\langle-\hat{\mu}^{s}_{\mathrm{eff}}\left[\vec{X}-\vec{X}'_{\mathrm{phot}}+2\left(R_b-\Delta r\right)\right]\right\rangle\end{array}\right\}\\ &= \frac{1}{4\pi D}\frac{1}{\left|\vec{X}-\vec{X}'_{\mathrm{phot}}\right|}\left\{\begin{array}{c}\exp\left(-\sqrt{s+\mu_a c}\frac{1}{\sqrt{Dc}}\left|\vec{X}-\vec{X}'_{\mathrm{phot}}\right|\right)\\ -\exp\left\langle-\sqrt{s+\mu_a c}\frac{1}{\sqrt{Dc}}\left[\left|\vec{X}-\vec{X}'_{\mathrm{phot}}\right|+2\left(R_b-\Delta r\right)\right]\right\rangle\end{array}\right\}\end{aligned} \tag{17}$$

And implementation of Eq. (8) with Eq. (17) leads to the time-resolved photon fluence rate measured at the surface of a spherical tissue domain whose size is significantly greater than the reduced scattering pathlength of the tissue in response to a spatially and temporally impulse photon source of unitary intensity within the tissue as the following:

$$\begin{aligned}\hat{\Psi}_{\mathrm{SOMA}}(\vec{\chi}', 0|\vec{\chi}, t) &= \frac{c}{(4\pi)^{3/2}}\frac{1}{[Dct]^{3/2}}\cdot\exp\left[-\mu_a ct\right]\\ &\cdot\left\langle\exp\left(-\frac{1}{4Dct}\left|\vec{X}-\vec{X}'_{\mathrm{phot}}\right|^2\right)-\exp\left\{-\frac{1}{4Dct}\left[\left|\vec{X}-\vec{X}'_{\mathrm{phot}}\right|+2\left(R_b-\Delta r\right)\right]^2\right\}\right\rangle\end{aligned} \tag{18}$$

Equation (18) is the temporal point-spread function or temporal impulse response of the spherical tissue medium for the evaluation of surface emission of time-resolved photons originating from the center of the spherical tissue domain.

4 Estimation of the temporal spread of light of spectral relevancy to induced PE in a spherical tissue volume of up to 40 cm in diameter due to photon diffusion

Equation (18) is implemented to assess the temporal spread of a light impulse of UPE spectral relevancy, after experiencing diffusion in a highly scattering tissue domain of 20 cm or 40 cm in diameter. The 40 cm diameter is not arbitrary, as it is comparable to the cross-sectional size of an adult human. The refractive index of the tissue is set as 1.40 which will reduce the speed of light in tissue to be 2.14×10^{-10} cm s^{-1}. Because tissue absorption does not contribute to the temporal spread, an absorption coefficient of $\mu_a = 0.1$ cm^{-1} that is representative of a bulk biological tissue at the Vis–NIR band [57] is assigned to the homogeneous tissue domain. The reduced scattering coefficient of the tissue is set at three values: 10 cm^{-1}, 100 cm^{-1} and 500 cm^{-1}. Among these three values of the reduced scattering coefficient, 10 cm^{-1} can be easily found for a biological tissue [57], but 500 cm^{-1} may be too strong to be associated with any biological tissues [58]. The temporal spread caused by an extremely strong reduced scattering coefficient of 500 cm^{-1} will thus safely set the upper limit of the temporal spread that cannot be surpassed by the photon diffusion process, when UPE photons have to traverse from a site of photogenesis within the tissue to a surface site of measurement.

The temporal spread function of Eq. (18) evaluated for the aforementioned sizes of the spherical tissue domains and values of reduced scattering coefficient is displayed in Fig. 3, after normalizing to the peak value of each. The (A) and (B) correspond to a tissue size of a radius of 10 cm or a diameter of 20 cm. The (C) and (D) refer to the tissue size of a radius of 20 cm or a diameter of 40 cm. The time-resolved photon fluence rate being the ordinate is displayed at a linear scale in (A) and (C), and a logarithmic scale in (B) and (D). The range of the ordinates representing the photon fluence rate (equivalently the photon count) in (B) and (D) is limited to ten orders of magnitude, which, however, well exceeds the experimental dynamic ranges (six orders of magnitude would be very common for a configuration with a fixed setting on gain or exposure time) of detecting induced PE [40]. Figure 3 demonstrates that, as photons of

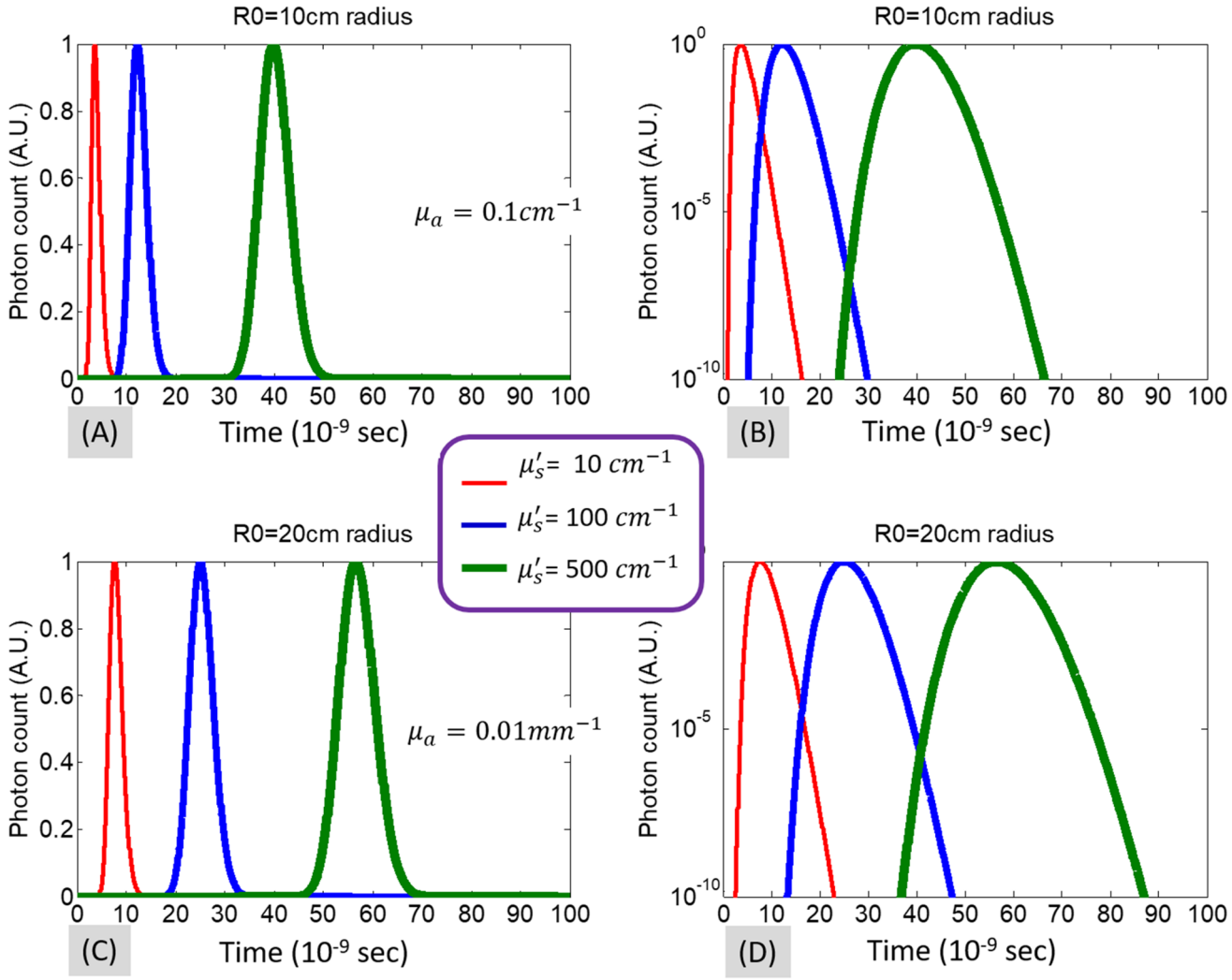

Fig. 3 Temporal spread of the photon fluence rate measured at the surface of a spherical tissue domain with an absorption coefficient of $\mu_a = 0.1$ cm^{-1} and at a reduced scattering coefficient of, respectively, [10, 100, 500] cm^{-1}, in response to a spatially and temporally impulsive source at the center of the spherical tissue domain. **a** Photon count (relative) at linear scale for a tissue volume of 10 cm in radius or 20 cm in diameter, **b** photon count (relative) at logarithmic scale for a tissue volume of 10 cm in radius or 20 cm in diameter, **c** photon count (relative) at linear scale for a tissue volume of 20 cm in radius or 40 cm in diameter, **d** photon count (relative) at logarithmic scale for a tissue volume of 20 cm in radius or 40 cm in diameter

UPE spectral relevancy diffuse in tissue over a line-of-sight distance of 20 cm that is comparable to the distance from the cross-sectional center of a human-size tissue to the cross-sectional edge, an extremely high values of tissue reduced scattering coefficient of 500 cm^{-1} that is about 50 times stronger than the reduced scattering coefficient of typical soft biological tissues will produce a temporal spread of less than 90 ns. The 90 ns spread equates to a total photon pathlength of less than 20 m in tissue. It is noted that this 90 ns maximal temporal spread is also associated with a dynamic range of ten orders of magnitude that is approximately four orders of magnitude greater than the instrument responses typical to the detection of induced PE. It can thus be projected that any photon emission of induced PE from organisms that has a delay time longer than 100 ns after the removal of the exogenous stress cannot be accounted for by only the temporal broadening of the photon pack due to tissue scattering. A slower phase of producing the photons then has to exist to make the elevation of the UPE above the baseline level of spontaneous emission to appear at a time much later than the delay caused by the tissue scattering, and a longer phase of producing the photons also has to be available for the induced PE to decay over a duration that is many orders of magnitude longer than the timescales of temporal broadening by tissue scattering.

5 Discussion

What this two-part work attempts to address is the need to consider both *the delay scale and decay kinetics* as the temporal characteristics of induced PE, in interpreting the temporal course of induced PE to facilitate mechanistic discovery and practical application. There are many observations indicating that the induced PE arises and exists long after the removal of the stress; therefore, analyzing the temporal course of induced PE with respect to the controllable stress is not merely an issue of the decay kinetics. Analyzing the temporal course of induced PE with respect to the controllable stress must not neglect the temporal delay between the moment of stress change and the moment of change of the surface PE. That delay or retardation may be caused by many factors, but it will contain the time it takes for the stress change to trigger the change of photogenesis, and the time it takes for the change in the photon production resulted from the perturbation to photogenesis to "propagate" to the surface to appear as the change in the surface-assessed photon count. The soliton mechanism may help account for the primary cause of a long temporal decay by sustaining the excited molecular states without transitioning to cause photogenesis. The soliton mechanism at present seems to be the most probable one to provide stable transport of charges in biological systems which do not dissipate their energy and can decay with photon yield only at special conditions. The soliton mechanism could dictate the stress-transfer phase at some conditions or for some organisms or tissues but is unlikely to be the only one contributing to the quantum yield of the delayed PE in responding to stress of all varieties and revealing temporal patterns of all kinds. Even for that responding to stress of only light nature, multiple sources of induced PE have been manifested by the complex time trends of the decaying patterns that were subjected to approximation by hyperbolic like multi-exponential patterns [40].

Assessing the scattering-limited delay or lifetime of photons detected as induced PE may be particularly important to the exploration of the cause of entopic phenomena such as phosphene which became historically notable as "light flashes" experienced during translunar flight [59] and has been reported from patients with cancer undergoing radiation therapy [60]. The light sensations of sometimes "bluish flashes" were likely a result of direct activation of retinal photoreceptors or visual pathway neurons by ionizing radiation [61]. Should the radiation-induced free radicals near retinal photoreceptors cause lipid peroxidation, chemiluminescence leading to the creation of bioluminescent photons would then be possible [60]. An alternative hypothesis has been suggested that the phosphenes may in part result from direct Cherenkov light production in the vitreous humor or retina of the eye which seems to be supported by recent experimental measurements [60]. Whichever the cause of the phosphene is, time-resolved measurements are necessary to resolve the temporal transduction processes between an external stimulation and the objective production or the subjective perception of the induced photons giving the "flash" sensation. Tissue scattering-limited photon lifetime will then be a parameter affecting the time resolution of the measurement at a human scale in acquiring fast events such as radiation-induced light sensation, of which the kinetic pattern remains outstanding and which may offer the insights to the underpinning stress-transfer pathway of induced PE that is not amenable to slow measurements.

The shortest delay time after removing the stress as reported for induced PE was 8.5 μs in responding to the removal of photic stimulation [39], whereas the longest delay time measured of induced PE after the removal of stress was at the order of hours in response to non-photic stress [45]. An 8.5 μs delay of continuous light presence in tissue of a refractive index of 1.4 corresponds to a total photon pathlength of 1.82×10^3 m—a dimension that is three orders of magnitude greater than the height of an adult human. Even scaling the shortest UPE delay one order smaller to compensate for the possible afterglow of the photo-stimulation instrument when turned off, a 0.85 μs delay of continuous light presence in tissue still means a total photon pathlength of 1.82×10^2 m in the tissue, which is at least 1000 times greater than the size of many organisms from which the induced PE was acquired. Unless there are mechanisms that delay the generation of the photons (e.g., the initiation of the presence of elevated number of photons in tissue) emitted as induced PE after turning off each specific external stress, it would be difficult to imagine that the observed large range of the delay time of induced PE is caused entirely by the large pathlength (or equivalently the long lifetime) of the UPE photons in the tissue after being generated, unless the biophotons may trigger secondary photon emission of similar characteristics. UPE photon is in the Vis–NIR spectral range that is relatively transparent to biological tissue. When a photon of Vis–NIR spectral band with low intensity appears in the tissue by either external injection or local production, the photon will have to propagate in tissue and experience scattering and absorbing events that collectively will attenuate the light intensity and diffuse the photon path. For time-resolved PE photon propagation or tissue transmission of the PE photon originating from a photon source that has a finite lifetime, the tissue scattering will also broaden the PE temporal profile because

of the mixing of ballistic photons with photons that have experienced different amounts of scattering events. It is therefore intuitive to compare the maximal temporal spread of photons that can be accounted for by tissue scattering when responding to an instantaneous photon production, against the shortest temporal delay of induced PE that has been experimentally observed. This comparison would help identify whether a photogenic mechanism preceding and much longer in lifetime than the lifetime of photon propagation in tissue is imperative to interpreting the very wide range of the temporal delays of induced PE measured on the tissue surface.

Analysis of time-resolved photon diffusion in an extremely scattering tissue over a domain as large as the cross section of human (40 cm in diameter) reveals that scattering-caused temporal spread or broadening of the photon pack when detected at the organism or tissue surface will not be broader or appear later than 100 ns. Therefore, any induced PE with a delay time much longer than 100 ns has to have a much slower process of photogenesis to account for the delay observed. The shortest delay time of induced PE of 8.5 μs is nearly two orders of magnitude longer than the upper limit of the temporal spreading of photon propagation in tissue that could be caused by tissue scattering alone. The delay time of induced PE is the temporal spread of the photons measured on the tissue surface with respect to the instant of stress removal. A temporal spread of photons that is much later and longer than that can be caused by scattering-associated photon diffusion can only be explained by a slower and longer (if not retarded) process of the photons being produced, since each photon of induced PE detected at the tissue surface comes from a source and the photons must have traversed through the tissue to the surface from that source. This speculation of the slower sourcing of the photons in responding to a stress that have traversed through the tissue to the surface for being detected as induced PE is conceptually illustrated in Fig. 4. The photons emitted by any source in tissue and reaching the site of detection at the surface may diffuse in tissue over a distance much longer than a ballistic line-of-sight path between the source position and the detector position due to tissue scattering; however, the scattering-caused temporal delay happens at light speed. This light-speed photon diffusion when associated with a slower or longer production of the photons at the source position may be the only way to feasibly cause the temporal profile of the surface-detected photons to change at a later time and over a longer duration, in the absence of any secondary photon-emission process that is perhaps difficult to suggest.

In the case of slow photon sourcing, the temporal profile of the photons measured at the tissue surface shall be the convolution of the source temporal profile with the temporal point-spread function $\hat{\Psi}_{\text{SOMA}}(\vec{\chi}', 0|\vec{\chi}, t)$ of the photon diffusion process. When the spatially impulsive source at $\vec{\chi}'$ is temporary spread as is represented by $q(\vec{\chi}', t) = \delta(\vec{\chi}')\mathbb{q}(t), t \geq 0$, the convolution results in the following:

$$\boxed{\hat{\Psi}_{\text{Delay}}(\vec{\chi}', 0|\vec{\chi}, t)} = \hat{\Psi}_{\text{SOMA}}(\vec{\chi}', 0|\vec{\chi}, t) \circledast q(\vec{\chi}', t) = \int_{-\infty}^{\infty} \hat{\Psi}_{\text{SOMA}}(\vec{\chi}', 0|\vec{\chi}, \tau).\mathbb{q}(t-\tau)d\tau \tag{19}$$

When the temporally spread source at $\vec{\chi}'$ is also spatially spread as represented by $q(\vec{\chi}', t) = \mathbb{Q}(\vec{\chi}')\mathbb{q}(t), t \geq 0$, the spatial convolution will also contribute to the composite temporal profile of the photons detected at the tissue surface as the following:

$$\boxed{\hat{\Psi}_{\text{Delay}}(\vec{\chi}', 0|\vec{\chi}, t)} = \hat{\Psi}_{\text{SOMA}}(\vec{\chi}', 0|\vec{\chi}, t) \circledast q(\vec{\chi}', t) = \int_{-\infty}^{+\infty} \mathbb{Q}(\vec{\chi}' - x) \cdot \left[\int_{-\infty}^{\infty} \hat{\Psi}_{\text{SOMA}}(x, 0|\vec{\chi}, \tau) \cdot \mathbb{q}(t-\tau)d\tau\right] dx \tag{20}$$

Equation (20) will be relevant if the spatial extent of the entity that may source the induced PE is known—a topic that is prohibiting at the present because of the lack of mechanistic discoveries. This work thus has limited the discussion of photogenesis to be spatially impulsive to estimate the contribution of the tissue scattering to the temporal profile of the photons that will be detected at the tissue surface as induced PE. For a temporal impulse response $\hat{\Psi}_{\text{SOMA}}(\vec{\chi}', 0|\vec{\chi}, t)$ that is significantly faster (i.e., 100 times faster) than the temporal profile of the source generation $q(\vec{\chi}', t) = \mathbb{q}(t)$, the temporal impulse response $\hat{\Psi}_{\text{SOMA}}(\vec{\chi}', 0|\vec{\chi}, t)$ can be approximated as a Dirac delta function for the convolution. And the temporal profile of the outcome of the convolution of any function with a Dirac delta function will be dictated by the temporal profile of the host function. In referring to the previous section and Fig. 3, one can find that the temporal spread expected for photons propagating over a line-of-sight distance of 20 cm in a tissue of extremely high reduced scattering coefficient of 500 cm^{-1} with a detection dynamic range of six orders of magnitude is in fact less than 80 ns. The shortest delay time of 8.5 μs of induced PE is > 100 times longer than the 80 ns temporal spread that is practically the upper limit of the temporal scale of $\hat{\Psi}_{\text{SOMA}}(\vec{\chi}', 0|\vec{\chi}, t)$. Therefore, the temporal profile of delayed photon acquisition at delay times longer than 8.5 μs will faithfully follow the temporal profile of the photon generation of $q(\vec{\chi}', t) = \mathbb{q}(t)$. For this reason, the analysis to be performed in the subsequent Part II, where

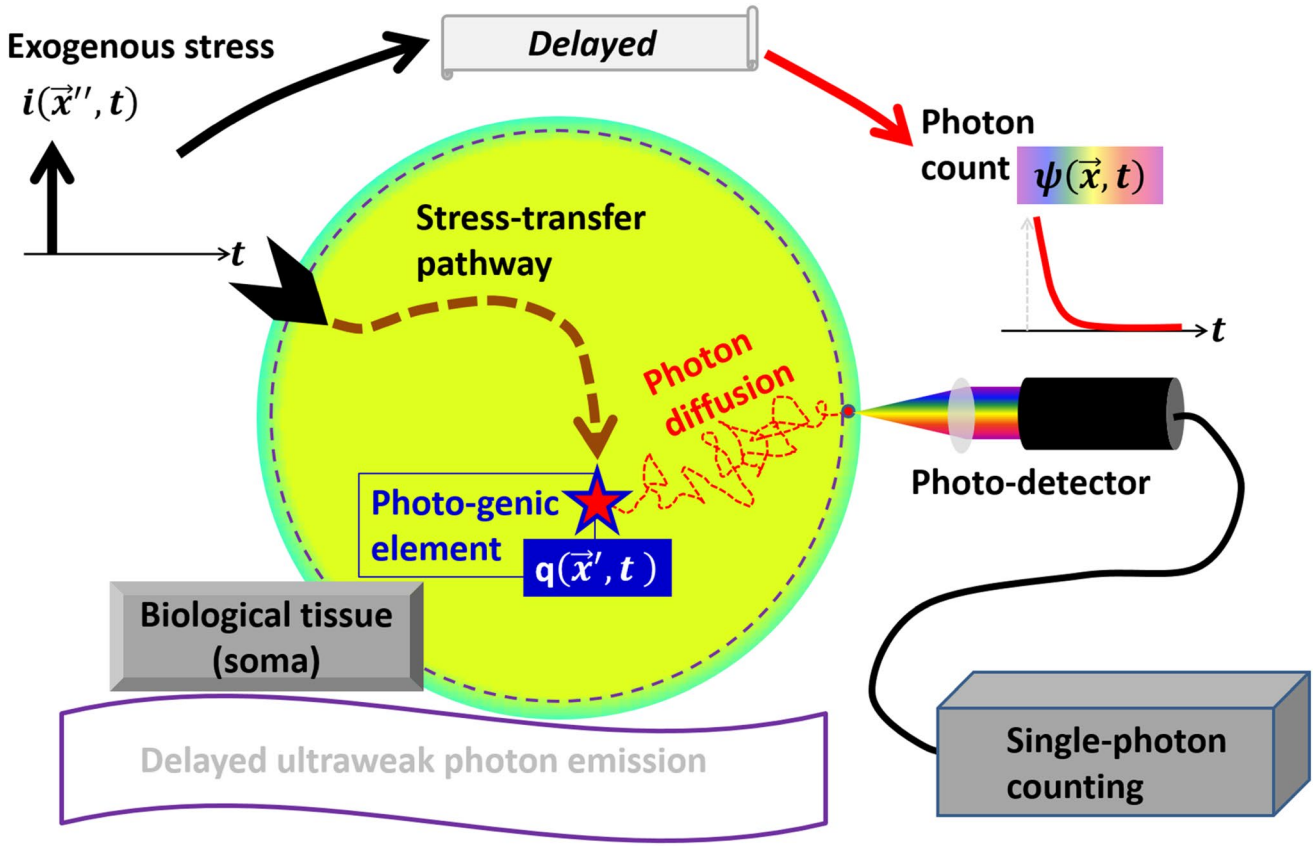

Fig. 4 A slower process of sourcing the photon generation in response to an external stress is necessary for making the surface-emitted photon to reveal a delay and the duration much longer than the time of light propagation in tissue due to the tissue scattering alone

a few stress-transfer pathways are modeled from a system perspective to project the decay patterns observed for induced PE, will be restricted to the kinetics of photogenesis of $q(\vec{x}', t) = \mathbb{q}(t)$.

6 Conclusion

Induced PE is usually substantially retarded in occurrence or longer in duration with respect to the stress. This work concerns that the surface emission of induced PE would involve light propagation in tissue whereby tissue scattering will set the minimal delay of the surface appearance of the photons of induced PE. This appreciation is pertinent to identifying the dominating temporal course of stress-induced PE from organism following stress of various types including but not limited to light. It is proposed that the surface emission of induced PE involves two causally sequential phases: a stress-transfer phase that transforms the stress to perturb photogenesis balanced at homeostasis and a photon-propagation phase that transmits the photons from the domain of perturbed photogenesis to surface emission. The traversing of induced PE photons from wherever the domains of photogenesis perturbation are in the organism following the stress to the surface must involve photon propagation of which the scattering will affect the photon lifetime. This Part I has theorized the maximal temporal delay of surface-emitted induced PE, with respect to the onset of photogenesis that is assumed to locate at the center of a spherical tissue volume of comparable in size to a human body, due to an unrealistically strong reduced scattering coefficient for assessing the longest possible temporal delay. Numerical implementation of the solution of time-resolved photon diffusion in the pertinent geometry found that tissue scattering alone will not cause more than 100 ns delay. The results suggest a much retarded and slower perturbation to photogenesis with respect to the time course of stress for manifesting the surface-observed induced PE as have been reported. The theoretical insight, which may complement the soliton mechanism in addressing the complex temporal characteristics of induced PE, also supports the exploration of entopic phenomena such as phosphenes and negative afterimages via delayed PE. The time course of induced PE seems to be attributable entirely to the stress-transfer process in the absence of secondary mechanism

to prolong the lifetime of photons after photogenesis. The subsequent Part II hypothesizes a few stress-transfer kinetic patterns feeding the photogenesis.

Acknowledgements The author wishes to thank the anonymous reviewers for their constructively specific comments.

Compliance with ethical standards

Conflict of interest The author declares that he has no conflict of interest.

References

1. Cifra M, Pospisil P (2014) Ultra-weak photon emission from biological samples: definition, mechanisms, properties, detection and applications. J Photochem Photobiol, B 139:2–10
2. Bokkon I, Salari V, Tuszynski JA, Antal I (2010) Estimation of the number of biophotons involved in the visual perception of a single-object image: biophoton intensity can be considerably higher inside cells than outside. J Photochem Photobiol, B 100(3):160–166
3. Kobayashi K, Okabe H, Kawano S, Hidaka Y, Hara K (2014) Biophoton emission induced by heat shock. PLoS ONE 9(8):e105700
4. Calcerrada M, Garcia-Ruiz C (2019) Human ultraweak photon emission: key analytical aspects, results and future trends—a review. Crit Rev Anal Chem 49:368–381
5. Oros CL, Alves F (2018) Leaf wound induced ultraweak photon emission is suppressed under anoxic stress: observations of Spathiphyllum under aerobic and anaerobic conditions using novel in vivo methodology. PLoS ONE 13(6):e0198962
6. Popp FA, Nagl W, Li KH, Scholz W, Weingartner O, Wolf R (1984) Biophoton emission. New evidence for coherence and DNA as source. Cell Biophys 6(1):33–52
7. Quickenden TI, Que Hee SS (1974) Weak luminescence from the yeast *Saccharomyces cerevisiae* and the existence of mitogenetic radiation. Biochem Biophys Res Commun 60(2):764–770
8. Cadenas E, Boveris A, Chance B (1980) Low-level chemiluminescence of bovine heart submitochondrial particles. Biochem J 186(3):659–667
9. Boveris A, Puntarulo SA, Roy AH, Sanchez RA (1984) Spontaneous chemiluminescence of soybean embryonic axes during imbibition. Plant Physiol 76(2):447–451
10. Devaraj B, Usa M, Inaba H (1997) Biophotons: ultraweak light emission from living systems. Curr Opin Solid State Mater Sci 2(2):188–193
11. Cohen S, Popp FA (1997) Biophoton emission of the human body. J Photochem Photobiol, B 40(2):187–189
12. Wang J, Yu Y (2009) Relationship between ultra-weak bioluminescence and vigour or irradiation dose of irradiated wheat. Luminescence 24(4):209–212
13. Havaux M, Triantaphylides C, Genty B (2006) Autoluminescence imaging: a non-invasive tool for mapping oxidative stress. Trends Plant Sci 11(10):480–484
14. Moraes TA, Barlow PW, Klingele E, Gallep CM (2012) Spontaneous ultra-weak light emissions from wheat seedlings are rhythmic and synchronized with the time profile of the local gravimetric tide. Naturwissenschaften 99(6):465–472
15. Zhang J, Yu W, Sun T, Popp FA (1997) Spontaneous and light-induced photon emission from intact brains of chick embryos. Sci China C Life Sci 40(1):43–51
16. Dotta BT, Saroka KS, Persinger MA (2012) Increased photon emission from the head while imagining light in the dark is correlated with changes in electroencephalographic power: support for Bokkon's biophoton hypothesis. Neurosci Lett 513(2):151–154
17. Wijk RV, Wijk EP (2005) An introduction to human biophoton emission. Forsch Komplement Klass Naturheilkd 12(2):77–83
18. Glaser AK, Zhang R, Davis SC, Gladstone DJ, Pogue BW (2012) Time-gated Cherenkov emission spectroscopy from linear accelerator irradiation of tissue phantoms. Opt Lett 37(7):1193–1195
19. Boveris A, Cadenas E, Reiter R, Filipkowski M, Nakase Y, Chance B (1980) Organ chemiluminescence: noninvasive assay for oxidative radical reactions. Proc Natl Acad Sci U S A 77(1):347–351
20. Cadenas E (1984) Biological chemiluminescence. Photochem Photobiol 40(6):823–830
21. Gallas JM, Eisner M (1987) Fluorescence of melanin dependence upon excitation wavelength and concentration. Photochem Photobiol 45(5):595–600
22. Kayatz P, Thumann G, Luther TT, Jordan JF, Bartz-Schmidt KU, Esser PJ, Schraermeyer U (2001) Oxidation causes melanin fluorescence. Invest Ophthalmol Vis Sci 42(1):241–246
23. Kalaji HM, Goltsev V, Bosa K, Allakhverdiev SI, Strasser RJ, Govindjee (2012) Experimental in vivo measurements of light emission in plants: a perspective dedicated to David Walker. Photosynth Res 114(2):69–96
24. Fedorova GF, Trofimov AV, Vasil'ev RF, Veprintsev TL (2007) Peroxy-radical-mediated chemiluminescence: mechanistic diversity and fundamentals for antioxidant assay. Arkivoc 8:163–215
25. Zhao X, Pang J, Fu J, Wang Y, Yang M, Liu Y, Fan H, Zhang L, Han J (2017) Spontaneous photon emission: a promising non-invasive diagnostic tool for breast cancer. J Photochem Photobiol, B 166:232–238
26. Kobayashi M, Iwasa T, Tada M (2016) Polychromatic spectral pattern analysis of ultra-weak photon emissions from a human body. J Photochem Photobiol, B 159:186–190
27. Wang Z, Wang N, Li Z, Xiao F, Dai J (2016) Human high intelligence is involved in spectral redshift of biophotonic activities in the brain. Proc Natl Acad Sci U S A 113(31):8753–8758
28. Slawinski J (1988) Luminescence research and its relation to ultraweak cell radiation. Experientia 44(7):559–571
29. Iyozumi H, Kato K, Makino T (2002) Spectral shift of ultraweak photon emission from sweet potato during a defense response. Photochem Photobiol 75(3):322–325
30. Slawinski J, Ezzahir A, Godlewski M, Kwiecinska T, Rajfur Z, Sitko D, Wierzuchowska D (1992) Stress-induced photon emission from perturbed organisms. Experientia 48(11–12):1041–1058
31. Musumeci F, Scordino A, Triglia A (1997) Delayed luminescence from simple biological systems. Riv Biol 90(1):95–110
32. Tsuchida K, Iwasa T, Kobayashi M (2019) Imaging of ultraweak photon emission for evaluating the oxidative stress of human skin. J Photochem Photobiol, B 198:111562
33. Salari V, Scholkmann F, Vimal RLP, Csaszar N, Aslani M, Bokkon I (2017) Phosphenes, retinal discrete dark noise, negative afterimages and retinogeniculate projections: a new explanatory framework based on endogenous ocular luminescence. Prog Retin Eye Res 60:101–119
34. Bokkon I, Vimal RL, Wang C, Dai J, Salari V, Grass F, Antal I (2011) Visible light induced ocular delayed bioluminescence as a possible origin of negative after image. J Photochem Photobiol, B 103(2):192–199
35. Wang C, Bokkon I, Dai J, Antal I (2011) Spontaneous and visible light-induced ultraweak photon emission from rat eyes. Brain Res 1369:1–9
36. Burgos RCR, Zhang W, van Wijk EPA, Hankemeier T, Ramautar R, van der Greef J (2017) Cellular glutathione levels in HL-60

cells during respiratory burst are not correlated with ultra-weak photon emission. J Photochem Photobiol, B 175:291–296
37. Burgos RCR, Schoeman JC, Winden LJV, Cervinkova K, Ramautar R, Van Wijk EPA, Cifra M, Berger R, Hankemeier T, Greef JV (2017) Ultra-weak photon emission as a dynamic tool for monitoring oxidative stress metabolism. Sci Rep 7(1):1229
38. Rac M, Sedlarova M, Pospisil P (2015) The formation of electronically excited species in the human multiple myeloma cell suspension. Sci Rep 5:8882
39. Niggli HJ, Tudisco S, Privitera G, Applegate LA, Scordino A, Musumeci F (2005) Laser-ultraviolet-A-induced ultraweak photon emission in mammalian cells. J Biomed Opt 10(2):024006
40. Baran I, Ionescu D, Privitera S, Scordino A, Mocanu MM, Musumeci F, Grasso R, Gulino M, Iftime A, Tofolean IT, Garaiman A, Goicea A, Irimia R, Dimancea A, Ganea C (2013) Mitochondrial respiratory complex I probed by delayed luminescence spectroscopy. J Biomed Opt 18(12):127006
41. Scordino A, Campisi A, Grasso R, Bonfanti R, Gulino M, Iauk L, Parenti R, Musumeci F (2014) Delayed luminescence to monitor programmed cell death induced by berberine on thyroid cancer cells. J Biomed Opt 19(11):117005
42. Goraczko W, Slawinski J (2004) Secondary ultraweak luminescence from humic acids induced by gamma-radiation. Nonlinearity Biol Toxicol Med 2(3):245–258
43. Maccarrone M, Fantini C, Agro AF, Rosato N (1998) Kinetics of ultraweak light emission from human erythroleukemia K562 cells upon electroporation. Biochim Biophys Acta 1414(1–2):43–50
44. Červinková MBLJMCK (2016) Low frequency electromagnetic field effects on ultra-weak photon emission from yeast cells. In: 2016 ELEKTRO
45. Volodyaev I, Beloussov LV (2015) Revisiting the mitogenetic effect of ultra-weak photon emission. Front Physiol 6:241
46. Jain A, Rieger I, Rohr M, Schrader A (2010) Antioxidant efficacy on human skin in vivo investigated by UVA-induced chemiluminescence decay analysis via induced chemiluminescence of human skin. Skin Pharmacol Physiol 23(5):266–272
47. Gu Q, Popp FA (1992) Nonlinear response of biophoton emission to external perturbations. Experientia 48(11–12):1069–1082
48. Kurian P, Obisesan TO, Craddock TJA (2017) Oxidative species-induced excitonic transport in tubulin aromatic networks: potential implications for neurodegenerative disease. J Photochem Photobiol, B 175:109–124
49. Voit F, Schafer J, Kienle A (2009) Light scattering by multiple spheres: comparison between Maxwell theory and radiative-transfer-theory calculations. Opt Lett 34(17):2593–2595
50. Ishimaru A (1989) Diffusion of light in turbid material. Appl Opt 28(12):2210–2215
51. Nakamura K, Hiramatsu M (2005) Ultra-weak photon emission from human hand: influence of temperature and oxygen concentration on emission. J Photochem Photobiol, B 80(2):156–160
52. Wojtkiewicz S, Durduran T, Dehghani H (2018) Time-resolved near infrared light propagation using frequency domain superposition. Biomed Opt Express 9(1):41–54
53. Arridge SR, Cope M, Delpy DT (1992) The theoretical basis for the determination of optical pathlengths in tissue—temporal and frequency-analysis. Phys Med Biol 37(7):1531–1560
54. Haskell RC, Svaasand LO, Tsay TT, Feng TC, McAdams MS, Tromberg BJ (1994) Boundary conditions for the diffusion equation in radiative transfer. J Opt Soc Am A Opt Image Sci Vis 11(10):2727–2741
55. Piao D, Barbour RL, Graber HL, Lee DC (2015) On the geometry dependence of differential pathlength factor for near-infrared spectroscopy. I. Steady-state with homogeneous medium. J Biomed Opt 20(10):105005
56. Piao DQ (2014) Photon diffusion in a homogeneous medium bounded externally or internally by an infinitely long circular cylindrical applicator. VI. Time-domain analysis. J Opt Soc Am A Opt Image Sci Vis 31(10):2232–2243
57. Jacques SL (2013) Optical properties of biological tissues: a review. Phys Med Biol 58(11):R37–R61
58. Yang Y, Wang T, Biswal NC, Wang X, Sanders M, Brewer M, Zhu Q (2011) Optical scattering coefficient estimated by optical coherence tomography correlates with collagen content in ovarian tissue. J Biomed Opt 16(9):090504
59. Fazio GG, Jelley JV, Charman WN (1970) Generation of Cherenkov light flashes by cosmic radiation within the eyes of the Apollo astronauts. Nature 228(5268):260–264
60. Tendler II, Hartford A, Jermyn M, LaRochelle E, Cao X, Borza V, Alexander D, Bruza P, Hoopes J, Moodie K, Marr BP, Williams BB, Pogue BW, Gladstone DJ, Jarvis LA (2020) Experimentally observed Cherenkov light generation in the eye during radiation therapy. Int J Radiat Oncol Biol Phys 106(2):422–429
61. Tobias CA, Budinger TF, Lyman JT (1971) Radiation-induced light flashes observed by human subjects in fast neutron, X-ray and positive pion beams. Nature 230(5296):596–598